**Atmospheric
Chemistry
and Physics
Discussions**

Modelling atmospheric structure, cloud and their response to CCN in the Central Arctic: ASCOS case studies

C. E. Birch[1], I. M. Brooks[1], M. Tjernström[2], M. D. Shupe[3], T. Mauritsen[4],
J. Sedlar[5], A. P. Lock[6], P. Earnshaw[6], P. O. G. Persson[3], S. F. Milton[6], and
C. Leck[2]

[1]Institute for Climate and Atmospheric Science, University of Leeds, Leeds, UK
[2]Department of Meteorology and the Bert Bolin Centre for Climate Research, Stockholm
University, Stockholm, Sweden
[3]University of Colorado, Boulder, CO, USA and NOAA-ESRL, Boulder, CO, USA
[4]Max Planck Institute for Meteorology, Hamburg, Germany
[5]Swedish Meteorological and Hydrological Institute, Norrköping, Sweden
[6]Met Office, Exeter, UK

Correspondence to: C. E. Birch (c.e.birch@leeds.ac.uk)

ACPD

12, 2559–2601, 2012

ASCOS case studies

C. E. Birch et al.

Title Page

Abstract | Introduction

Conclusions | References

Tables | Figures

◄ | ►

◄ | ►

Back | Close

Full Screen / Esc

Printer-friendly Version

Interactive Discussion

Abstract

Observations made during late summer in the Central Arctic Ocean, as part of the Arctic Summer Cloud Ocean Study (ASCOS), are used to evaluate cloud and vertical temperature structure in the Met Office Unified Model (MetUM). The observation period can be split into 5 regimes; the first two regimes had a large number of frontal systems, which were associated with deep cloud. During the remainder of the campaign a layer of low-level cloud occurred, typical of Central Arctic summer conditions, along with two periods of greatly reduced cloud cover. The short-range operational NWP forecasts could not accurately reproduce the observed variations in near-surface temperature. A major source of this error was found to be the temperature-dependant surface albedo parameterisation scheme. The model reproduced the low-level cloud layer, though it was too thin, too shallow, and in a boundary-layer that was too frequently well-mixed. The model was also unable to reproduce the observed periods of reduced cloud cover, which were associated with very low cloud condensation nuclei (CCN) concentrations ($< 1\,\mathrm{cm}^{-3}$). As with most global NWP models, the MetUM does not have a prognostic aerosol/cloud scheme but uses a constant CCN concentration of $100\,\mathrm{cm}^{-3}$ over all marine environments. It is therefore unable to represent the low CCN number concentrations and the rapid variations in concentration frequently observed in the Central Arctic during late summer. Experiments with a single-column model configuration of the MetUM show that reducing model CCN number concentrations to observed values reduces the amount of cloud, increases the near-surface stability, and improves the representation of both the surface radiation fluxes and the surface temperature. The model is shown to be sensitive to CCN only when number concentrations are less than 10–$20\,\mathrm{cm}^{-3}$.

Title Page

Abstract | Introduction

Conclusions | References

Tables | Figures

◀◀ | ▶▶

◀ | ▶

Back | Close

Full Screen / Esc

Printer-friendly Version

Interactive Discussion

1 Introduction

Arctic temperatures are increasing faster than the global mean (Manabe and Wetherald, 1975; Serreze and Barry, 2011) and this is projected to continue through the 21st century (ACIA, 2004; Holland et al., 2006; Solomon et al., 2007). Sea ice extent and
5 thickness have also decreased (Nghiem et al., 2007; Comiso et al., 2008; Parkinson and Cavalieri, 2008), and the period 2007 to 2011 has seen the lowest September extents in the satellite record (NSIDC, 2011). Processes that occur in the Arctic are also linked to both global ocean and atmospheric circulations and thus changes in the Arctic climate system are expected to have an impact at lower latitudes. Sea ice extent
10 has been found to influence weather patterns in the Northern Hemisphere (Alexander et al., 2004; Deser et al., 2007; Bhatt et al., 2008; Overland et al., 2010), such as the Pacific storm track (Chapman and Walsh, 2007) and cold winter weather over Eurasia (Francis et al., 2009). For all these reasons it is important to accurately represent Arctic meteorological processes in global models, both for weather prediction and to project
15 changes in Arctic climate.

Climate models are used extensively to make projections of future climate. However, there are large differences between individual model predictions, especially related to the magnitude and spatial patterns of the warming and to the extent and timing of the reduction in sea ice (Arzel et al., 2006; Serreze and Francis, 2006). The links between
20 Arctic processes and weather systems at lower latitudes (Deser et al., 2007; Alexander et al., 2004; Bhatt et al., 2008) mean that seasonal and sub-seasonal forecasts for mid-latitudes in the Northern Hemisphere are also currently limited by poor representation of the Arctic. These uncertainties result, at least in part, from the lack of detailed understanding of processes specific to the Arctic region. Many of the physical processes
25 involving the ocean, sea ice, snow cover, clouds and radiation occur on spatial and temporal scales not explicitly resolved by global climate models. They must instead be parameterised as functions of resolved-scale model parameters. The quality and the sensitivity of any climate model is critically dependent on how this is done. Although

conditions can differ greatly from those in mid-latitudes, there are few parameterisations specific to the Arctic; largely because it is so difficult to make the extensive in-situ observations necessary to develop new parameterisations.

Clouds have a pronounced influence on the Arctic surface energy budget (Curry et al., 1996; Shupe and Intrieri 2004; Sedlar et al., 2011a) and thus on the melting and freezing of the Arctic perennial sea ice (Kay and Gettelman, 2009; Persson, 2011). In spite of this importance, clouds remain an Achilles heel in our understanding of the climate system and consequently in climate modelling (e.g., Solomon et al., 2007). This is particularly true for Arctic clouds (Walsh et al., 2002; Tjernström et al., 2008; Karlsson and Svensson, 2010). During the summer months a persistent layer of low-level stratiform cloud exists over sea ice in the Central Arctic Ocean (Intrieri et al., 2002; Tjernström et al., 2004; Tjernström, 2007). Intrieri et al. (2002) and Shupe et al. (2011) show that the annual cloud fraction peaked at almost 100 % during August and September during the Surface Heat Budget of the Arctic (SHEBA) experiment (Uttal et al., 2002). Low-level clouds ($< 2\,\mathrm{km}$) were the most common during this period, occurring at least 50 % of the time. The low-level clouds were most frequently mixed-phase, although a significant number of liquid-only clouds occurred (Shupe, 2011). Similar conditions were also observed at Barrow, Alaska, although the peak in total cloud fraction and low-level cloud occurs approximately one month later in the year.

Since clouds are important in regulating the region's surface energy budget (Curry et al., 1996; Shupe and Intrieri 2004; Sedlar et al., 2011a), it is essential to understand processes relating to the formation and persistence of these clouds in order to develop parameterisations to accurately represent them. The position of a cloud in a vertical profile is closely tied to the vertical temperature structure of the atmosphere (Norris, 1998). A temperature inversion in the Arctic is common during all seasons between the surface and altitudes of 1–2 km, which has become known as the "Arctic inversion" (Kahl et al., 1990, 1992; Serreze et al., 1992; Kahl and Martinez, 1996; Tjernström and Graversen, 2009). Sedlar and Tjernström (2009) show that during late summer only 30 % of cloud tops are coincident with the temperature inversion base, as found in

ASCOS case studies

C. E. Birch et al.

Full Screen / Esc

Printer-friendly Version

Interactive Discussion

marine stratocumulus at lower latitudes (Paluch and Lenschow, 1991; Stevens et al., 2007). In the remaining cases cloud top was found well inside the inversion (Sedlar and Tjernström, 2009; Sedlar et al., 2011b); a feature that is unique to the Arctic pack ice region and important for cloud persistence (Solomon et al., 2011).

Birch et al. (2009) present a general evaluation of a recent version of the Met Office Unified Model (MetUM) using data from the Arctic Ocean Experiment (AOE) 2001 (Tjernström et al., 2004). They concluded that the occurrence and radiative properties of deeper clouds, which are associated with frontal systems, are represented more accurately than the low-level cloud that is ubiquitous to the summer Central Arctic boundary layer. Models generally produce a layer of low-level cloud but there are large inter-model differences and the occurrence of relatively clear periods is underestimated (Tjernström et al., 2008). Model difficulties in simulating low-level Arctic cloud may be related to a model's inability to resolve the Arctic inversion (Tjernström et al., 2008) or to maintain supercooled liquid water (Morrison and Pinto 2005; Solomon et al., 2009).

Cloud formation requires both water vapour saturation and the presence of cloud condensation nuclei (CCN), which provide a surface on which water can condense. Lannerfors et al. (1993), Bigg et al. (1996), Bigg and Leck (2001), Leck et al. (2002) and Mauritsen et al. (2011) present observations of summer CCN number concentrations over the Arctic pack ice region from various field campaigns. During the Arctic Summer Ocean Cloud Study (ASCOS), the observed CCN concentrations were usually a few $10\,s\,cm^{-3}$, rarely as high as $100\,cm^{-3}$, and sometimes less than $1\,cm^{-3}$. This is in contrast to lower latitudes where typical concentrations range from approximately $100\,cm^{-3}$ to several $1000\,cm^{-3}$ in the marine environment (Raes et al., 2000). Such low CCN number concentrations mean cloud droplet size spectra, and hence radiative properties, will differ from those at mid-latitudes. Mauritsen et al. (2011) argue that cloud formation is frequently limited by CCN availability in the Central Arctic. They use the term "tenuous cloud regime" to describe this circumstance, which occurs between the usual situation where the aerosol needed to form cloud are in abundance, and

Title Page

Abstract | Introduction

Conclusions | References

Tables | Figures

◄◄ | ►►

◄ | ►

Back | Close

Full Screen / Esc

Printer-friendly Version

Interactive Discussion

a hypothetical situation, where there are no aerosol and therefore condensation does not occur except at very high supersaturations ($\sim 400\%$ relative humidity).

Here we use observations from the ASCOS field campaign to assess how well a global numerical model (MetUM) represents the low-level temperature structure and cloud observed over the Arctic pack ice. An example of a tenuous cloud regime is then used to highlight one possible reason why models over-predict low-level cloudiness.

2 ASCOS observations

ASCOS took place on the Swedish icebreaker *Oden* during August and early September 2008. The ship departed Svalbard on 2 August (day of year (DoY) 215) and, after a few short observation periods in the open ocean and marginal ice zone, cruised north until a suitable ice floe was located at 87°21′ N and 01°29′ W on 12 August (DoY 225) (Fig. 1). The floe was approximately 3×6 km and was surrounded by a mixture of open leads and other ice floes of various sizes. The ship was moored to the floe and drifted with it for the duration of the ice research station, which was in operation between 13 August (DoY 226) and 1 September (DoY 245). *Oden* then sailed south, returning to Svalbard on 9 September (DoY 253).

Two meteorological masts were placed on the ice floe during the ice station. Air temperature, pressure, relative humidity and high frequency 3-D wind measurements were made from these masts at multiple heights above the surface. Unobstructed observations of long and shortwave radiation fluxes were made on the ice floe using broadband radiometers, and surface temperature measurements were made with an array of eight thermocouples. A more detailed description of this instrumentation can be found in Sedlar et al. (2011a).

Radiosondes (Vaisala RS92), providing profiles of temperature, relative humidity, and wind speed and direction, were launched from the helipad of the icebreaker four times a day at approximately 00:00, 06:00, 12:00 and 18:00 UTC for the entire duration of the cruise. This amounted to 86 soundings during the ice drift period and 145

soundings in total. Each profile was subsequently interpolated onto a uniform set of vertical levels that ranged from 5 m vertical resolution in the lowest 1 km of the troposphere to 100 m in the stratosphere.

A suite of remote sensing instruments were installed on-board *Oden* and were oper-
5 ational for almost the entire duration of the cruise. These included a 35-GHz millimeter cloud radar (MMCR; Moran et al., 1998), several laser ceilometers, a scanning 60 GHz radiometer, a dual wavelength (24/31 GHz) microwave radiometer (MWR, Westwater et al., 2001), an S-band cloud and precipitation radar, and a 449 MHz wind profiler. Estimates of cloud liquid and ice water concentrations were derived by combining data
10 from a number of these instruments. The first step was to classify cloud phase using radar reflectivity, mean Doppler velocity and spectral width from the MMCR, vertical temperature profiles from the radiosondes, and liquid water path (LWP) derived from the MWR (Shupe, 2007). LWP can be diagnosed relatively easily from the MWR, with a root mean square error of approximately $25 \, \mathrm{g\,m^{-2}}$ (Westwater et al., 2001). Liquid
15 cloud properties were then derived from the cloud phase classification, the LWP, the radiosonde vertical temperature profiles, cloud base derived from the ceilometer and cloud top derived from the MMCR. Ice cloud properties were derived using the MMCR radar reflectivity-based retrievals with an Arctic specific retrieval coefficient and the cloud phase classification (Shupe et al., 2005, 2006).

20 The vertical extent of liquid layers (i.e. cloud top and base) and the LWP can be retrieved with reasonable accuracy during periods without precipitation, but the relative vertical distribution within the cloud layers is uncertain and assumed to be adiabatic. In contrast to the liquid properties, the relative vertical distribution of ice within the cloud boundaries is well diagnosed from radar reflectivity, but the total ice water path (IWP)
25 is not. The uncertainty in the magnitude of IWP could be up to a factor of two, and is due to a combination of both systematic and random error. This should be borne in mind during comparisons with the model.

Particle number size distributions and CCN number concentrations were measured in-situ onboard *Oden*. CCN were measured with two identical CCN counters (Roberts

and Nenes, 2005). One counter used a constant supersaturation of approximately 0.2 %, while the other cycled between 0.1 and 0.7 %. The former instrument was used to obtain CCN number concentrations relevant for low-level stratocumulus cloud formation and the latter was used to identify cases when the CCN number concentration estimate was particularly sensitive to the choice of supersaturation (Martin et al., 2011). Air for sampling was drawn in via a sampling manifold located at approximately 25 m above sea level. An Anderson impactor with a 10 μm diameter particle cut size was located at the inlet of the manifold. A pollution sensor prevented direct contamination from the ship exhaust. Particle size distributions with diameters between 3 nm to 10 μm were continuously monitored, with a time resolution of 10 to 20 min. Two differential mobility analyzers (DMAs) were deployed to measure the number size distributions of dry sub-micrometer particles. The transfer functions of the DMAs and the size-dependent counting efficiencies of both condensation particle counters were calibrated before the campaign. For more details on the sampling manifold, the pollution sensor and on the number particle size distributions see Heintzenberg and Leck (2011).

3 Met Office Unified Model

This study uses the global numerical weather prediction (NWP) version of the Met Office Unified Model (MetUM) (Davies et al., 2005; Staniforth et al., 2006). Since the MetUM can be run on a range of temporal scales, it is well suited for use as a tool to infer systematic errors in the parameterisations of climate models (Phillips et al., 2004) when suitable measurements are available for only short periods of time. The observations can be used to evaluate model processes at the scale of individual weather systems where the large-scale synoptic flow in the model is well constrained by data assimilation.

The first set of model diagnostics used in this study were derived from the operational NWP global forecasts that were generated during the ASCOS field campaign (model cycle G48). Model data sets are comprised of 12-h operational forecasts, updated by

00:00 UTC and 12:00 UTC analyses and sampled at 3-h forecast intervals ($t + 15$, 18, 21, 24 h). The 3-hourly diagnostic data from every forecast are then concatenated to produce a continuous data series from 13 August to 2 September 2008 (DoY 226 to 246), to cover the entire ice drift period. For each 3-h forecast interval, model diagnostics from the grid box containing the ship's location were selected for comparison with the observations. This method of analysis involves the evaluation of grid box averaged model data against point observations. Some care must be taken interpreting such comparisons since, for at least some variables, the two may represent rather different physical properties (see Birch et al., 2009, for a more detailed discussion).

A single-column model (SCM) version of the Met Office Unified Model is also utilised in this study. The SCM contains the same physical parameterisations as the global version of the model, but the larger-scale dynamics can be constrained using the ASCOS observations. It is a useful tool for running experiments with different initialisations or model options to compare with the observations. To run a SCM simulation of the entire ice camp period, the advective terms for temperature, humidity and wind need to be known. It is not possible to acquire these terms from single 6-hourly radiosonde profiles. Instead, a separate 6-h SCM run is initialised with wind, temperature, pressure and humidity profiles from each of the 6-hourly radiosondes and additional surface temperature measurements. The advective terms are assumed to be zero over the 6-h runs. The ice-surface albedo is also initialised at $\alpha = 0.75$, which is representative of that observed. This is to reduce the effect of the surface-temperature bias caused by the Unified Model's temperature-dependent surface albedo parameterisation scheme (see Birch et al., 2009).

Model cycle G48 has semi-Lagrangian, semi-implicit and non-hydrostatic formulations (Davies et al., 2005) and a 4D-Var data assimilation system (Rawlins et al., 2007). The operational global NWP horizontal resolution is 0.375° latitude by 0.5625° longitude. The model resolves variables on a staggered grid, where dynamical (winds and pressure) and thermodynamical variables are at different levels. The lowest thermodynamic levels are at 20, 80, 180, 320 and 500 m. The radiation scheme is based on

the two-stream equations in both the longwave and shortwave spectral regions follow-ing Edwards and Slingo (1996). It allows for consistency in physical processes that are important in both spectral regions, such as overlapping cloud layers and includes the treatment of the effects of non-spherical ice particles and allows multiple scattering between cloud layers and the surface. The surface-flux scheme is based on Monin-Obukhov similarity theory and surface fluxes are computed following Louis (1979).

The cloud scheme is based on Smith (1990) but includes a cloud/precipitation mi-crophysical scheme with prognostic ice (Wilson and Ballard, 1999), based on Rutledge and Hobbs (1983). Cloud liquid water content and fractional area are determined di-agnostically by assuming a triangular probability distribution function of subgrid mois-ture, with the width given by a prescribed value of relative humidity. Ice cloud fractional area is calculated assuming a similar diagnostic relationship between the ice water con-tent and the ice cloud fraction. As a result there is no direct link between the relative humidity and ice cloud; it is the assumptions in the large-scale precipitation scheme (Wilson and Ballard, 1999) that govern the balance between water vapour and ice. Ice nucleation can only occur at temperatures colder than −10 °C and ice cloud water content can also be advected. The total volume cloud fraction is calculated assuming minimum overlap between ice and liquid cloud.

Although the MetUM can be run as a fully coupled ocean-atmosphere model, both NWP versions used here have fixed sea ice fractions, derived from satellite observa-tions. At the latitudes relevant to ASCOS, the model assumes 100 % sea ice cover and sea ice thickness is also constant, at 2 m. The SCM is run with the same prescribed sea ice characteristics. The effects of surface leads and melt ponds on albedo and turbulent fluxes are not included in the model parameterisations, though these were both present.

Observations from the ASCOS radiosonde launches were not submitted to the Global Telecommunications System, and hence were not utilised in the MetUM op-erational forecast and data assimilation cycle. The soundings therefore represent in-dependent validation data, as do the cloud retrievals and surface observations. There

are few, if any, in-situ observations from the Central Arctic Ocean assimilated into the operational forecasts, although satellite retrievals of wind and radiance are assimilated at very low vertical resolution.

4 Overview of conditions observed during ASCOS

Near-surface air temperature, wind speed, pressure and surface albedo observed during the ice drift period of the field campaign and forecast by the MetUM are shown in Fig. 2. There is good agreement between the observed and modelled pressure and wind speed, which suggests the larger-scale dynamics are well represented in the model.

The ice drift period can be split into five regimes using the near-surface air temperature, surface energy budget, vertical structure and synoptic conditions (Tjernström et al., 2011). The observed temperature is close to 0 °C until DoY 234. This initial period, designated as one single regime by Sedlar et al. (2011a), can be divided into two regimes; a period that saw high winds and the passage of a large number of frontal systems (1st regime, DoY 226.0 to 229.5), followed by a period of lower wind speeds and fewer frontal passages (2nd regime DoY 229.5 to 234.0). The near-surface air temperature dropped to −7 °C in the 3rd regime (DoY 234.0 and 236.4), then increased to between −4 and −2 °C in the 4th regime (DoY 236.4 to 244.75), before dropping rapidly to −13 °C in the 5th (DoY 244.75 to 246.0). The role of cloud and the surface energy budget in this temporal development is described in detail by Sedlar et al. (2011a).

The model near-surface air temperature shows less correlation with the observations than the wind speed or pressure. The model is equal to, or warmer than, the observations during all regimes apart from a 5-day period in the 4th regime. Even in the 1st and 2nd regimes, the model fails to reproduce the small decreases in temperature associated with passing synoptic features, which is partly due to a known issue with the surface albedo parameterisation in the operational version of the Met Office Unified Model (Birch et al., 2009). The albedo parameterisation is temperature dependent;

when the ice surface temperature is at 0 °C, the albedo is set to the minimum value of 0.5. The albedo increases linearly with decreasing surface temperature to a maximum of 0.8 at −10 °C. Birch et al. (2009) show that this causes a significant feedback, where high surface temperatures cause the albedo to be too low, which maintains the bias in surface temperature.

The observations of albedo were made over a small area (∼ 10 m by 10 m) of snow and ice surface and are therefore not representative of a model grid box, which should include an open lead and melt pond fraction. Although the fraction of melt ponds and open leads varied during the ice camp, a rough estimate of albedo for a grid box-size area can be derived using the approximate ice (80 %) and open water (20 %) surface fractions estimated from aerial photographs that were taken at the beginning of the ice camp, when the ice and melt fraction was at its maximum (not shown). In reality the true albedo will lie somewhere between the observations and the estimated spatial average because the fraction of melt ponds and leads significantly decreased during the observation period. Cogley (1979) show that for direct radiation, the albedo of water increases with increasing solar zenith angle. The solar zenith angle is always relatively large during the summer months in the Central Arctic, but because there is a near-persistent cloud layer the amount of direct radiation incident on the surface is small. For these reasons a value of 0.04 is assumed for the open water albedo and is used along with the approximate fractions of ice and open water to compute an estimate of the spatially averaged albedo. The observed surface albedo, the computed "grid box" estimate and the model surface albedo are shown in Fig. 2d. The "grid box" estimate is lower than the observed albedo but both illustrate that the albedo increased during the ice camp period, which was caused by new snowfall onto the older, darker ice. The "grid-box" estimate between DoY 236 and 246 represents an extreme lower limit because by this period of the melt-to-freeze transition, the fraction of open leads and melt ponds was significantly lower than 20 %. The model reproduces this trend because the model surface temperature generally decreases over the ice camp period (snowfall does not have an impact on surface albedo in the model). However, there

is a large negative bias in model albedo. This result holds regardless of whether the comparison is made with the true observations or the estimated spatial average.

The bias in model surface albedo is reflected in the positive temperature bias during the 1st and 2nd regimes and also has an influence on the biases in the 3rd and 5th regimes. In the 4th regime there is a transition from a positive to a negative bias in the model temperature on DoY 239. This is caused by a combination of errors in the surface albedo parameterisation scheme and cloud cover. During the second half of DoY 238 the model produces a clear period, which is not seen in the observations (Fig. 3). This allows the surface to cool strongly by the emission of longwave radiation and thus decreases the temperature of the surface, which in turn increases the albedo from its minimum of 0.5. Subsequently, surface temperatures lower than those observed persist until the end of the 4th regime.

Liquid, ice and total cloud water concentrations observed during ASCOS and the equivalent diagnostics from the MetUM are shown in Fig. 3. The passages of a large number of deep frontal systems during the 1st and 2nd regimes, and one at the beginning of the 4th regime, are seen in the observations. The timing of these periods of deep frontal cloud is reproduced reasonably well in the model. One notable difference during this period is that the liquid in the model clouds extends to only 3 km above the surface, compared to 6 km in the observations. Also, the amount of ice in the deep, frontal clouds appears to be much lower in the model than in the observations. Some, but not all, of this bias may result from the factor of two uncertainty in the magnitude of the retrievals of ice water concentrations.

At the beginning of the 3rd regime, the surface pressure begins to increase (Fig. 2) and there are no frontal systems that pass the observation site. Another front passes the site at the beginning of the 4th regime. This is followed by a low-level layer of cloud for the rest of the 4th regime. Periods of reduced cloudiness occur during the 3rd and 5th regimes. The low-level clouds have a much lower ice water content than the deeper frontal clouds in the first part of the observation period, but have significant liquid water contents. The model reproduces the low-level cloud but has too low a liquid water

content, and generally both too thin and at too low an altitude. The model does not reproduce the periods of reduced cloud cover in the 3rd and 5th regimes.

5 Atmospheric stability

Figure 4 gives an overview of the observed and modelled temperature structure of the
lower atmosphere during each regime. Radiosonde data and equivalent diagnostics from the MetUM were used to compute the static stability, given by the vertical derivative of equivalent potential temperature as a function of height ($\partial\theta_e/\partial z$). Probability distributions are shown for each regime. The observations show that the 1st regime was mostly well-mixed in the lowest 4 km, which was associated with strong winds,
numerous fronts and cyclonic systems. The main inversion in the 2nd regime was between 200 and 500 m above the surface and the variability in the lowest 500 m was much greater than in the 1st regime. The 4th regime has a more distinct inversion between 500 m and 1 km, with most often well-mixed conditions below and weakly stable above. In the 3rd and 5th regimes the inversion extends from the surface up to 800 m.
In the model there is much less variation in stability between the 5 regimes (right column in Fig. 4): the main inversion resides between approximately 500 m and 1 km in all cases, and the stability below this is too frequently well-mixed.

The SCM can be used to test whether the MetUM can maintain more accurate stability profiles if given accurate initial conditions. The observations, averaged onto the
model vertical grid resolution and the SCM results at $t + 6$ h are shown in the first and second columns of Fig. 5. Since the SCM was initialised with the observations, the model diagnostics at $t + 0$ h are identical to the observations. Comparing the observations to the model diagnostics at $t + 6$ h indicates the ability of the model to maintain the observed stability profile. The SCM diagnostics at $t + 6$ h show much more resem-
blance to the observations than the diagnostics from the operational forecasts (Fig. 4). The height of the main inversion base is much closer to that observed in all regimes except the 5th. However, the lowest 500 m is still too well-mixed relative to the observed

profiles. Even when the model is initialised with observed profiles, which represent a range of stabilities in the lowest 500 m, after 6 h of integration the variability has significantly decreased. This is particularly apparent in the 1st, 2nd and 4th regimes. The SCM is initialised with a strong inversion near the surface in the 3rd and 5th regimes and even this strong stability is reduced in the model after 6 h.

The most significant model biases in stability occur within the lowest 1 km of the atmosphere, which corresponds to just 7 vertical levels in the MetUM. It is possible that there are not enough vertical levels in the model to reproduce the surface-based mixed layer, cloud layer and main inversion that are observed. An experiment was performed in which the vertical resolution of the SCM was increased to 50 m throughout the full profile. This allows for 20 vertical levels in the lowest 1 km, compared to 7 in the standard configuration. The radiosonde observations, averaged onto a 50 m vertical grid, and the results from the SCM simulation are shown in the third and fourth columns of Fig. 5, respectively.

The behaviour of the SCM at 50 m vertical resolution is very similar to that at the standard resolution. The height of the main inversion layers in the 1st, 2nd and 4th regimes are similar to those observed and similar to the SCM runs with standard vertical resolution. The lowest 500 m of the model becomes well mixed within the first 6 h of the simulations, which shows that increasing the vertical resolution of the model from 5 to 10 levels in the lowest 500 m does not improve the vertical structure. The lowest 100 m of the model is well-mixed too frequently during the 3rd regime in the SCM runs with standard vertical resolution because it forms a cloud layer when the observations suggest it is clear (similar to the NWP results in Fig. 3). Increasing the model vertical resolution to 50 m intervals increases the number of levels in the lowest 250 m from 3 to 5. In the SCM runs with increased vertical resolution the cloud layer that develops is deeper (not shown) and the erroneous near-surface well-mixed layer extends up to 250 m rather than 100 m. Similar errors appear in the 5th regime; the increased resolution causes the cloud layer to increase in altitude and the SCM becomes too well-mixed between 150 and 300 m, rather than between 300 m and the surface.

6 Case study – 4th regime

6.1 Cloud occurrence and stability

The low-level cloud and periods of reduced cloudiness during the 3rd, 4th and 5th regimes are more representative of the conditions that usually prevail during the summer months in the Central Arctic Ocean (Shupe et al., 2011) than the periods of deep, frontal cloud observed during the 1st and 2nd regimes. In addition, Birch et al. (2009) showed that, in the Arctic, model biases associated with low-level cloud are larger than those associated with the deep, frontal clouds. For these reasons the remainder of the study focuses on the 4th and 5th regimes, where the 4th is an example of a period with low-level cloud and the 5th is an example of a period with much reduced cloud cover.

Figure 6 shows the observed and modelled total cloud water concentrations for the 4th and 5th regimes. The model cloud layer is too thin, at too low an altitude, and the water concentrations are too low by approximately 30 %. The black dashed line in Fig. 6a represents the base of the strongest temperature inversion, found using the 6-hourly radiosonde observations and an automated algorithm. The algorithm indentifies an inversion as any layer with a positive temperature gradient; however, since temperature profiles from radiosonde observations are quite variable, objective criteria are implemented to distinguish between meteorologically significant inversions and shallower, more spurious ones (Tjernström and Graversen, 2009). All inversions below 3 km are identified and then sorted according to strength (by largest temperature gradient within each inversion). Inversions that are shallower than 20 m are discarded and any remaining inversions that are separated by less than 100 m are merged. The main inversion is defined as the inversion with the largest temperature gradient, as diagnosed by the algorithm. This algorithm is also applied to the model temperature profiles to gain an equivalent measure of height of main inversion base (Fig. 6b). The red line in each of the panels represents the top of the surface-based mixed layer, which was diagnosed subjectively using the θ_e profiles from the radiosonde observations and model diagnostics.

The top of the observed cloud layer is located near the main inversion, although it is generally not capped by it. In the model the cloud layer generally resides below the main inversion. As an example, Fig. 6c shows observed and model vertical profiles of total cloud water and θ_e at DoY 242.25. In the observations the main inversion base is at approximately 875 m but the cloud layer extends up to 1 km. The cloud layer in the model resides on the lowest four model levels and is capped by the main inversion, which begins at the 4 th model level (320 m). During some periods (e.g., DoY 242.5) the model cloud layer extends more than 200 m (but typically only one grid-level) into the main inversion. The penetration of cloud into the stable inversion appears to be similar to that observed in low-level Arctic clouds by Sedlar and Tjernström (2009) and Sedlar et al. (2011b). Given the model's coarse vertical grid, however, it is unlikely the model is correctly capturing the microphysical and turbulent processes. More likely it is simply the initial condensation in the grid-level above the cloudy mixed layer as it deepens (the inversion base rises between DoY 242.5 and 243.0).

For much of the time, the observed surface-based mixed layer only extends up to approximately 100 m and is therefore below the layer of cloud. This implies that the cloud may be decoupled from the surface. A separate mixed layer ($\partial\theta_e/\partial z \approx 0$) forced by cloud-top radiative cooling (e.g., Fig. 6c and Solomon et al., 2011) is located within the observed cloud. For most of the period, the modelled main inversion base and the top of the surface-based mixed layer coincide (Fig. 6b and example in Fig. 6c), likely resulting from the too low clouds producing a radiatively forced mixed layer that is too close to the surface. Hence, unlike the observations, the model cloud is coupled to the surface.

6.2 Initialisation and development of the cloud layer

Figure 7a–e shows total cloud water concentrations from six operational forecasts ($t + 3$ to $t + 96$ h), initialised at 12:00 UTC each day between DoY 236 and 241 (all within the 4th regime). Comparing these longer-range forecasts with the shorter-range $t + 15$ to $t + 24$ h forecasts in Fig. 6b highlights some further issues. In Fig. 7b–e the cloud

develops over the 4-day forecast from being adjacent to the surface to elevated above it. This development is highlighted in Fig. 7h–l, which indicates a general trend of increased cloud-layer height with time. Note that the symbols in Fig. 7h–l mark the heights of the vertical levels in the model; the model cloud resides on only two or three of these levels.

As the model time since initialisation increases we expect the vertical structure of the cloud layer to drift away from that specified by the analysis, towards a model-dependent preferred state. The results in Fig. 7 suggest that the preferred state of the model at $t + 96$ h is more similar to the observations than the model analyses (indicated by the $t + 15$ to $t + 24$ h forecasts in Fig. 6a). This suggests that something in the model forecast-assimilation-analysis cycle may be reducing the accuracy of the short-term forecasts.

There are few, if any, in-situ observations from the Central Arctic available for assimilation into operational forecast models. The only observations that are assimilated by the MetUM are satellite observations of wind and radiance, which are at a very coarse vertical resolution in the lower atmosphere. One would expect that the assimilation of any good quality observations into a model would increase the accuracy of the forecasts. However, the results of this study show that the model forecast-assimilation-analysis cycle actually reduces the accuracy of short-term forecasts, which suggests either that the satellite observations are not of sufficient quality or that the assimilation process itself introduces a bias. An investigation into data assimilation is beyond the scope of this paper but is recommended for future research.

Figure 7m–r shows the model vertical velocity for each of the $t + 3$ to $t + 96$ forecasts. Subsidence of up to $0.03\,\mathrm{m\,s^{-1}}$ occurs above 1 km in all the forecasts between DoY 239 to 242. The height of cloud top is determined by a balance between the subsidence and the entrainment rate (Lenderink and Holtslag, 2000), both of which are relatively small in magnitude. The effect of modifying this balance is illustrated by the change in vertical velocity from negative to positive on DoY 242; the model cloud layer begins to increase in altitude (Fig. 7c–e). There is also an increase in the height of the main

inversion base in the observations (DoY 242.75, Fig. 6a), which suggests the ascent that is resolved in the model occurred in reality.

Another example is the period of ascent in the model is between DoY 237.75 to 238.25. During this time a cloud between 2 and 3 km appears in the observations and the main inversion base, as determined by the automatic algorithm, is defined at 3 km rather than within the cloud layer that is situated below 500 m (Fig. 6a). In the model, the height of the main inversion base rises until DoY 238.75 (Fig. 6b and 7a,b), at which point there is an abrupt change to descent in the vertical velocity field. The model cloud disappears (Fig. 6b and 7a,b). Without the cloud the model surface cools, the temperature drops to 4 °C below that observed and the surface albedo increases (DoY 239, Fig. 2). The surface temperature does not fully recover to equal that observed until DoY 244, consistent with the increase in albedo. When the model cloud reappears at DoY 239.2 (Fig. 6b and 7a–c) the near-surface layer is stable (not shown) and therefore the cloud is only able to develop in the lowest 200 m of the atmosphere. In the longer-range forecasts (Fig. 7a–c) the cloud layer mixes upwards but it takes 2 to 3 days for cloud-top to reach 500 m. The upward mixing occurs even during a period of subsidence in the model (DoY 238.5 to 241.0), which means that the entrainment rate must by greater than the subsidence rate. An imbalance of 2 to 3 mm s^{-1} could cause approximately 200 m day^{-1} of cloud-top height change. It is not possible to test this with the ASCOS measurements.

7 CCN and cloud: the tenuous cloud regime

Figure 6 shows that the model produced low-level cloud during the 5th regime (DoY 244.75 to 246.0), when the observations show a period of much reduced cloud cover. This error in cloud cover is associated with model biases in near-surface air temperature (Fig. 2) and atmospheric stability (Fig. 4). Even when the SCM is initialised with radiosonde observations, within 6 h of the start of the run the near-surface stable layer becomes well-mixed (bottom row of Fig. 5). Here we examine these biases in more

detail.

Figure 8a shows cloud radar reflectivity observations during the 5th regime. The cloud almost entirely disappears at approximately DoY 244.8, returns briefly between DoY 245.4 and 245.7, before clearing again in the evening of DoY 245. Sedlar et al. (2011a) discuss this period in detail and show that the reduction in cloudiness causes the surface to cool via a significant imbalance of the upward and downward long-wave radiation fluxes at the surface (Fig. 8b), reducing the surface temperature by about 6 °C and initiating the onset of the autumn freeze-up. The reduction in cloud occurs at the same time as the CCN concentration and accumulation mode aerosol (60 nm < diameter < 800 nm) number concentrations fall below $1\,cm^{-3}$ (Fig. 8c). Mauritsen et al. (2011) studied this event in detail and argue that the cloud layer is greatly reduced during DoY 245 because the CCN number concentration is too low to maintain it; they term this the "tenuous cloud" regime.

The operational NWP and SCM versions of the MetUM do not have a prognostic aerosol/CCN scheme but assume a constant CCN concentration of $100\,cm^{-3}$ over all marine environments (including over sea-ice). The summary of observations by Mauritsen et al. (2011) suggests that CCN concentrations in the summertime Central Arctic seldom reach this value and are lower than $10\,cm^{-3}$ for 10–30 % of the time. The unrealistically high CCN number concentrations in the model may prevent the observed reduction in cloud cover during the 5th regime and explain the persistence of cloud in the operational forecasts during this period. Additional SCM simulations were performed with standard vertical resolution and constant CCN concentrations of 50, 20, 10, 5, 2 and $1\,cm^{-3}$ to test this hypothesis.

The results for the control and a selection of the CCN experiments at 23:30 UTC, DoY 244 and 05:40 UTC, DoY 245, are shown in Fig. 9. The mean observed CCN concentrations at these times are 0.50 and $0.35\,cm^{-3}$, respectively. The minimum value that can be defined in the SCM is $1\,cm^{-3}$, but this should adequately represent this period. The blue lines show static stability, liquid-water content and relative humidity with respect to water from the SCM runs at the time of initialisation ($t + 0$), and are

Full Screen / Esc

Printer-friendly Version

Interactive Discussion

representative of the observed values. At the time of both radiosonde launches the sky was almost entirely free of cloud and there was a stable layer throughout the lowest 100 m of the atmosphere caused by radiative cooling at the surface. In the control case (CCN = 100 cm^{-3}) a layer of cloud appears within the first six hours of the simulation and persists for at least 6 h (green lines). Associated with this, the stability close to the surface changes to near-neutral and the relative humidity becomes 100 %. When the CCN concentration is reduced to 20 cm^{-3}, the cloud that evolves in the model contains less liquid water than in the standard model run. The liquid cloud water concentration is even lower in the runs in which the CCN concentration is reduced to 5 cm^{-3}. The lowest 400 m of the atmosphere is more stable and the relative humidity is below 100 %. The best model results are produced when the CCN concentration is reduced to 1 cm^{-3}. The liquid cloud water concentration is very low, the relative humidity is below 100 % and the near-surface stability remains at approximately 0.04 K m^{-1}.

A change in model cloud inevitably alters the long and shortwave radiative fluxes at the surface. Figure 10 compares the observed surface radiative fluxes, averaged between 00:50 and 06:00 UTC, DoY 245, with the diagnostics at $t + 6$ h from the SCM runs initialised at 23:30 UTC, DoY 244 with CCN concentrations of 100, 20, 5, 2 and 1 cm^{-3}. The observed fluxes suggest that whilst the surface absorbs energy from the shortwave flux, the net flux is negative due to strong longwave cooling. When the model CCN concentration is between 100 and 20 cm^{-3}, the net longwave is almost zero, producing a positive net radiative flux. This explains why the model near-surface air temperature is too high during the 5th regime (Fig. 2). When the CCN concentration is less than 5 cm^{-3} the cloud layer in the model is significantly reduced, the downward shortwave flux increases and the surface cools through the emission of longwave radiation. As the CCN concentration is reduced from 5 to 1 cm^{-3}, the longwave emission becomes increasingly dominant and the net radiation flux agrees well with that observed.

The effect of improvements to the radiation budget is highlighted in the model surface temperature diagnostic. Figure 11 shows surface temperature observations from

each of the 8 thermocouples, along with their mean. The large coloured dots represent the surface temperature in the SCM at $t + 6$ h for each CCN concentration. The temperatures in the SCM runs with high CCN concentrations are positively biased because longwave cooling of the surface is limited by the cloud layer. Reducing the CCN concentration to 20 cm^{-3} makes only a small difference to this bias. It appears that the model is only sensitive to the number of CCN when the concentration is less than about 10–20 cm^{-3}. This is consistent with the results of Mauritsen et al. (2011) who found that the longwave cloud forcing is strongly sensitive to CCN concentration below about 10 cm^{-3}. When the CCN number concentration is reduced to 1 or 2 cm^{-3}, which is similar to the concentrations observed during this period, the model is able to maintain the tenuous cloud conditions and the model surface temperature is very close to that observed.

8   Summary and conclusions

Observations made during late summer in the Central Arctic Ocean pack ice area as part of ASCOS are used to evaluate the cloud and vertical temperature structure in the global operational NWP version of the Met Office Unified Model (MetUM). The period of observations was split into five regimes, based on the temperature, wind speed, pressure and cloud observations. The model reproduces the deep cloud associated with the passage of frontal systems (1st and 2nd regimes) with more success than the low-level cloud and intermittent cloud reductions that are ubiquitous to the Arctic pack ice area during summer (3rd, 4th and 5th regimes). The operational NWP forecasts produce cloud in the 4th regime that is too thin and resides in a boundary layer that is too shallow and too well-mixed, and remains coupled to the surface. The observations however, suggest that the cloud is usually decoupled from the surface. Increasing the vertical resolution of the model to 50 m does not reduce these biases, although it is possible that further increasing the vertical resolution in the lowest 500 m would show some improvements. The height of the cloud layer in the model appears to be partly

|◄ | ►|

◄ | ►

Back | Close

Full Screen / Esc

controlled by the large-scale ascent/subsidence; both observed and model cloud-top height increase during periods of model ascent.

The MetUM exhibits the tendency to become rapidly well-mixed and cloudy even when initialised with stably stratified conditions. This error is particularly apparent during the 5th regime; a cloud layer develops which is not observed, the model is too well-mixed near the surface, and the surface and near-surface temperatures are too high. Our results suggest that the model erroneously produces cloud during this period because it has a fixed CCN concentration of $100\,\mathrm{cm}^{-3}$ over all marine environments and is therefore unable to represent the low aerosol and CCN number concentrations that were observed during this period and caused the reduced cloud cover. Experiments with the MetUM single-column model show that reducing the CCN number concentration to $1\,\mathrm{cm}^{-3}$, close to that observed during the 5th regime, greatly reduces the cloud cover and improves the model surface radiative fluxes and temperature during the 5th regime.

It is important to accurately represent the timing of the melt transitions in climate models because they control the length of the melt season, which in turn affects the length of time ice melts in a given year (Perovich et al., 2007; Persson 2011). This study illustrates two modelling problems that need to be corrected in order for models to be able to realistically capture the end of the summer melt transition. Firstly, the processes changing the surface albedo must be correctly parameterized and large biases in the surface albedo must be removed. Such process errors can produce significant net energy flux errors of tens of $\mathrm{W\,m}^{-2}$, leading to timing errors in the net surface energy budget and the melt season transition. Secondly, errors affecting the downwelling longwave radiation must be identified and corrected. The results from this study suggest that correct and time-varying CCN number concentrations may be necessary to correctly reproduce the occurrence of Arctic stratocumulus clouds, and hence the downwelling radiation because Arctic CCN concentrations are often low enough to provide a significant sensitivity for cloud generation. Varying the CCN number concentration in the model shows that the model is only significantly sensitive to CCN number

concentrations below approximately 10–20 cm^{-3}. The inability of models to capture the low CCN, tenuous cloud regime is one possible explanation for why models the underestimate the occurrence of relatively clear periods (Tjernström et al., 2008).

The CCN observations made during four expeditions to the Arctic pack ice area during summer, summarised in Mauritsen et al. (2011), suggest that the CCN number concentration over the Central Arctic Ocean is less than 10 cm^{-3} 10–30 % of the time during summer. If the tenuous cloud regime always occurs when CCN number concentrations are low, the regime is important during a significant fraction of the summer season. With observations limited to four short expeditions that covered only a small region of the pack ice area, it is currently unclear how significant these events really are for the Arctic climate system. It must however be recognised that even if infrequent, the tenuous cloud event that was observed during ASCOS played a significant role in the transition from the summer melt season to freeze-up (Sedlar et al., 2011a), at least within the region in which ASCOS was located.

This study suggests that (a) improving surface albedo parameterisations and (b) implementing prognostic aerosol schemes within global models might improve the representation of Arctic cloud, the surface energy budget, and boundary-layer structure. Recent studies have produced surface-albedo parameterisations that depend on more realistic processes than that represented by just the surface temperature. Some of these schemes consider not only snowfall, but freezing of melt ponds, snow crystal metamorphosis, and spectral variations (e.g., Pedersen et al., 2009; Flocco et al., 2010). We recommend that these types of schemes be tested and incorporated in any model expecting to provide realistic results in the Arctic environment. Since 2003, the UK Met Office and its collaborators have been working to build and evaluate a state-of-the-art chemistry and aerosols model within the MetUM: the UK Chemistry and Aerosols (UKCA) model. One of the outcomes of this project will be the ability to run the MetUM in NWP mode with a prognostic aerosol/CCN scheme, which includes the interactions between aerosol and clouds. Work is already underway in evaluating aerosol and CCN number concentrations over the Central Arctic Ocean in the aerosol component

of UKCA (Global Model of Aerosol Processes, GLOMAP, Mann et al., 2010). Once this work is completed, GLOMAP or UKCA embedded in the MetUM will provide a useful tool for further research into the CCN-limited regime discussed in this study. The models will be useful in the assessment of the frequency and extent of the tenuous cloud regime, its impacts on climate and how it may change in the future.

References

ACIA: Impacts of a Warming Arctic: Arctic Climate Impact Assessment, Cambridge University Press, New York, USA, 2004.

Alexander, M. A., Bhatt, U. S., Walsh, J. E., Timlin, M., and Miller, J. S.: The atmospheric response to realistic Arctic sea ice anomalies in an AGCM during winter, J. Climate, 17, 890–905, 2004.

Arzel, O., Fichefet, T., and Goosse, H.: Sea ice evolution over the 20th and 21st centuries as simulated by current AOGCMs, Ocean Model., 12, 401–415, 2006.

Bhatt, U. S., Alexander, M. A., Deser, C., Walsh, J. E., Miller, J. S., Timlin, M. S., Scott, J. D., and Tomas, R. A.: The atmospheric response to realistic reduced summer Arctic sea ice

ASCOS case studies

C. E. Birch et al.

Title Page

Abstract	Introduction
Conclusions	References
Tables	Figures

◄ ► | ►►

◄ | ►

Back | Close

Full Screen / Esc

anomalies, in Arctic sea ice decline: observations, projections, mechanisms, and implications, Geophys. Mono. Ser., 180, 91–110, 2008.

Bigg, E. K. and Leck, C.: Cloud-active particles over the Central Arctic Ocean, J. Geophys. Res., 106, 32155–32166, 2001.

Bigg, E. K., Leck, C., and Nilsson, E. D.: Sudden changes in arctic atmospheric aerosol concentrations during summer and autumn, Tellus B, 48, 254–271, 1996.

Birch, C. E., Brooks, I. M., Tjernström, M., Milton, S. F., Earnshaw, P., Söderberg, S., and Persson, P. O. G.: The performance of a global and mesoscale model over the Central Arctic Ocean during late summer, J. Geophys. Res., 114, D13104, doi:10.1029/2008JD010790, 2009.

Chapman, W. L. and Walsh, J. E.: Simulations of Arctic temperature and pressure by global coupled models, J. Climate, 20, 609–632, 2007.

Cogley, J. G.: The albedo of water as a function of latitude, Mon. Weather Rev., 107, 775–781, 1975

Comiso, J. C., Parkinson, C. L., Gersten, R., and Stock, L.: Accelerated decline in the Arctic sea ice cover, Geophys. Res. Lett., 35, L01703, doi:10.1029/2007GL031972, 2008.

Curry, J., Rossow, W., Randall, D., and Schramm, J.: Overview of Arctic cloud and radiation characteristics, J. Climate, 9, 1731–1764, 1996.

Davies, T., Cullen, M. J. P., Malcolm, A. J., Mawson, M. H., Staniforth, A., White, A. A., and Wood, S.: A new dynamical core for the Met Office's global and regional modelling of the atmosphere, Q. J. Roy. Meteorol. Soc., 131, 1759–1782, 2005.

Deser, C., Thomas, R. A., and Peng, A.: The transient atmospheric circulation response to Northern Atlantic SST and sea ice anomalies, J. Climate, 20, 4751–4767, 2007.

Edwards, J. M. and Slingo, A.: Studies with a flexible new radiation code. I: Choosing a configuration for a large-scale model, Q. J. Roy. Meteorol. Soc., 122, 689–719, 1996.

Francis, J. A., Chan, W., Leathers, D. J., Miller, J. R., and Veron, D. E.: Winter Northern Hemisphere 565 weather patterns remember summer Arctic sea-ice extent, Geophys. Res. Lett., 36, L07503, doi:10.1020/2009GL037 274, 2009.

Flocco, D., Feltham, D. L., and Turner, A. K.: Incorporation of a physically based melt pond scheme into the sea ice component of a climate model, J. Geophys. Res., 115, C08012, doi:10.1029/2009JC005568, 2010.

Heintzenberg, J. and Leck, C.: The summer aerosol in the Central Arctic 1991–2008: did it change or not?, Atmos. Chem. Phys. Discuss., 12, 887–933, doi:10.5194/acpd-12-887-2012,

ASCOS case studies

C. E. Birch et al.

Title Page

Abstract	Introduction
Conclusions	References
Tables	Figures

◄ | ►

◄ | ►

Back | Close

Full Screen / Esc

Printer-friendly Version

Interactive Discussion

2012.

Holland, M. M., Bitz, C. M., and Tremblay, L.: Future abrupt reductions in the summer Arctic sea ice, Geophys. Res. Lett., 22, L23503, doi:10.1029/2006GL028024, 2006.

Intrieri, J., Fairall, C. W., Shupe, M., Persson, P., Andreas, E., Guest, P., and Moritz, R.: An annual cycle of Arctic surface cloud forcing at SHEBA, J. Geophys. Res., 107, C19, 8039, doi:10.1029/2000JC000439, 2002.

Kahl, J. D.: Characteristics of the low-level temperature inversion along the Alaskan Arctic coast, Int. J. Climatol., 10, 537–548, 1990.

Kahl, J. D. and Martinez, D. A.: Long-term variability in the low-level inversion layer over the Arctic Ocean, Int. J. Climatol., 16, 1297–1313, 1996.

Kahl, J. D., Serreze, M. C., and Schnell, R. C.: Tropospheric low-level temperature inversions in the Canadian Arctic, Atmos. Ocean, 30, 511–529, 1992.

Karlsson, J. and Svensson, G.: The simulation of Arctic clouds and their influence on the winter surface temperature in present-day climate in the CMIP3 multi-model dataset, Clim. Dyn., 36, 623–635, 2010.

Kay, J. E. and Gettelman, A.: Cloud influence on and response to seasonal Arctic sea ice loss, J. Geophys. Res., 114, D18204, doi:10.1029/2009JD011773, 2009.

Lannerfors, H., Heintzenberg, J., and Hansson, H.-C.: A comprehensive study of physical and chemical parameters of the Arctic summer aerosol results from the Swedish expedition Ymer-80, Tellus B, 35, 40–54, 1983.

Leck, C., Norman, M., Bigg, E. K., and Hillamo, R.: Chemical composition and sources of the high Arctic aerosol relevant for fog and cloud formation, J. Geophys. Res., 107, D12, 4135, doi:10.1029/2001JD001463, 2002.

Lenderink, G. and Holtslag, A. A. M.: Evaluation of kinetic energy approach for modeling turbulent fluxes in stratocumulus, Mon. Weather Rev., 128, 244–258, 2000.

Louis, J. F.: A parametric model of vertical eddy fluxes in the atmosphere, Bound.-Layer Meteorol., 17, 187–202, 1979.

Manabe, S. and Wetherald, R. T.: The effects of doubling the CO_2 concentration in the climate of a general circulation model, J. Atmos. Sci., 32, 3–15, 1975.

Mann, G. W., Carslaw, K. S., Spracklen, D. V., Ridley, D. A., Manktelow, P. T., Chipperfield, M. P., Pickering, S. J., and Johnson, C. E.: Description and evaluation of GLOMAP-mode: a modal global aerosol microphysics model for the UKCA composition-climate model, Geosci. Model Dev., 3, 519–551, doi:10.5194/gmd-3-519-2010, 2010.

Title Page

Abstract | Introduction

Conclusions | References

Tables | Figures

◄ | ►

◄ | ►

Back | Close

Full Screen / Esc

Printer-friendly Version

Interactive Discussion

Martin, M., Chang, R. Y.-W., Sierau, B., Sjogren, S., Swietlicki, E., Abbatt, J. P. D., Leck, C., and Lohmann, U.: Cloud condensation nuclei closure study on summer arctic aerosol, Atmos. Chem. Phys., 11, 11335–11350, doi:10.5194/acp-11-11335-2011, 2011.

Mauritsen, T., Sedlar, J., Tjernström, M., Leck, C., Martin, M., Shupe, M., Sjogren, S., Sierau, B., Persson, P. O. G., Brooks, I. M., and Swietlicki, E.: An Arctic CCN-limited cloud-aerosol regime, Atmos. Chem. Phys., 11, 165–173, doi:10.5194/acp-11-165-2011, 2011.

Moran, K. P., Martnew, B. E., Post, M. J., Kropfli, R. A., Welsh, D. C., and Widener, K. B.: An unattended cloud-profiling radar for use in climate research, B. Am. Meteorol. Soc., 79, 443–455, 1998.

Morrison, H. and Pinto, J. O.: Mesoscale modeling of springtime arctic mixed-phase stratiform clouds using a new two-moment bulk microphysics scheme, J. Atmos. Sci., 62, 3683–3704, 2005.

Nghiem, S. V., Rigor, I. G., Perovich, D. K., Clemente-Colón, P., and Weatherly, J. W.: Rapid reduction of Arctic perennial sea ice, Geophys. Res. Lett., 34, L19504, doi:10.1029/2007GL031138, 2007.

Norris, J. R.: Low cloud type over the ocean from surface observations, Part I: relationship to surface meteorology and the vertical distribution of temperature and moisture, J. Climate, 11, 369–382, 1998.

NSIDC: Arctic sea ice new and analysis: Summer 2011: Arctic sea ice near record lows, National Snow and Ice Data Centre, available at: http://nsidc.org/arcticseaicenews/, accessed 4 October 2011.

Overland, J. E. and Wang, M.: Large-scale atmospheric circulation changes are associated with the recent loss of Arctic sea ice, Tellus A, 62, 1–9, 2010.

Paluch, I. R. and Lenschow, D. H.: Stratiform cloud formation in the marine boundary layer, J. Atmos. Sci., 48, 2141–2158, 1991.

Parkinson, C. L. and Cavalieri, D. J.: Arctic sea ice variability and trend, 1979–2006, J. Geophys. Res., 113, C07004, doi:10.1029/2007JC004564, 2008.

Perovich, D. K., Nghiem, S. V., Markus, T., and Schweiger, A.: Seasonal evolution and inter-annual variability of the local solar energy absorbed by the Arctic sea ice-ocean system, J. Geophys. Res., 112, C03005, doi:10.1029/2006JC003558, 2007.

Pedersen, C. A., Roeckner, E., Lüthje, M., and Winther, J.-G.: A new sea ice albedo scheme including melt ponds for ECHAM5 general circulation model, J. Geophys. Res., 114, D08101, doi:10.1029/2008JD010440, 2009.

Title Page

Abstract | Introduction

Conclusions | References

Tables | Figures

◄ | ►

◄ | ►

Back | Close

Full Screen / Esc

Printer-friendly Version

Interactive Discussion

Perovich, D. K., Nghiem, S. V., Markus, T., and Schweiger, A.: Seasonal evolution and inter-annual variability of the local solar energy absorbed by the Arctic sea ice-ocean system, J. Geophys. Res., 112, C03005, doi:10.1029/2006JC003558, 2007.

Persson, P. O. G.: Onset and end of summer melt season over sea ice: thermal structure and surface energy perspective from SHEBA, Clim. Dyn., doi:10.1007/s00382-011-1196-9, 2011.

Phillips, T. J., Potter, G. L., Williamson, D. L., Cederwall, R. T., Boyle, J. S., Fiorino, M., Hnilo, J. J., Olson, J. G., Xie, S., and Yio, J.: Evaluating parameterizations in General Circulation Models, B. Am. Meteorol. Soc., 85, 1903–1915, 2004.

Raes, F., Van Dingenen, R., Vignati, E., Wilson, J., Putaud, J. P., Seinfeld, J. H., and Adams, P.: Formation and cycling of aerosols in the global troposphere, Atmos. Env., 34, 4215–4240, 2000.

Rawlins, F., Ballard, S. P., Bovis, K. J., Clayton, A. M., Li, D., Inverarity, G. W., Lorenc, A. C., and Payne, T. J.: The Met Office Global 4-dimensional variational data assimilation scheme, Q. J. Roy. Meteorol. Soc., 133, 347–362, 2007.

Roberts, G. C. and Nenes, A..: A continuous-flow streamwise thermal-gradient CCN chamber for atmospheric measurements, Aerosol Sci. Technol., 39, 206–221, 2005.

Rutledge, S. A. and Hobbs, P. V.: The mesoscale and microscale structure and organization of clouds and precipitation in midlatitude cyclones, VIII: a model for the "seeder-feeder" process in warm-frontal rainbands, J. Atmos. Sci., 40, 1185–1206, 1983.

Sedlar, J. and Tjernström, M.: Stratiform cloud-inversion characterization during the Arctic melt season, Bound.-Layer Meteorol., 132, 455–474, 2009.

Sedlar, J., Tjernström, M., Mauritsen, T., Shupe, M. D., Brooks, I. M., Persson, P. O. G., Birch, C. E., Leck, C., Sirevaag, A., and Nicolaus, M.: A transitioning Arctic surface energy budget: the impacts of solar zenith angle, surface albedo and cloud radiative forcing, Clim. Dyn., 37, 7–8, 1643–1660, doi:10.1007/s00382-010-0937-5, 2011a.

Sedlar, J., Shupe, M. D., and Tjernström, M.: On the relationship between thermodynamic structure and cloud top, and its climate significance in the Arctic, J. Climate, in press, doi:10.1175/JCLI-D-11-00186.1, 2011b.

Serreze, M. C. and Barry, R. G.: Processes and impacts of Arctic amplification: a research synthesis, Global Plant. Change, 77, 85–96, 2011.

Serreze, M. C. and Francis, J.: The Arctic amplification debate, Clim. Change, 76, 241–264, 2006.

Title Page

Abstract | Introduction

Conclusions | References

Tables | Figures

◄ | ►

◄ | ►

Back | Close

Full Screen / Esc

Printer-friendly Version

Interactive Discussion

Serreze, M. C., Kahl, J. D., and Schnell, R. C.: Low-level temperature inversions of the Eurasian Arctic and comparisons with Soviet drifting station data, J. Climate, 5, 615–629, 1992.

Shupe, M. D.: A ground-based multiple remote-sensor cloud phase classifier, Geophys. Res. Lett., 34, L22809, doi:10.1029/2007GL031008, 2007.

Shupe, M. D.: Clouds at Arctic atmospheric observations. Part II: Thermodynamic phase characteristics, J. Appl. Meteorol. Clim., 50, 645–661, 2011.

Shupe, M. D. and Intrieri, J. M.: Cloud radiative forcing of the Arctic surface: the influence of cloud properties, surface albedo, and solar zenith angle, J. Climate, 17, 616–628, 2004.

Shupe, M. D., Uttal, T., and Matrosov, S. Y.: Arctic cloud microphysics retrievals from surface-based remote sensors, J. Appl. Meteorol., 44, 1544–1562, 2005.

Shupe, M. D., Matrosov, S. Y., and Uttal, T.: Arctic mixed-phase cloud properties derived from surface-based sensors at SHEBA, J. Atmos. Sci., 63, 697–711, 2006.

Shupe, M. D., Walden, V. P., Eloranta, E., Uttal, T., Campbell, J. R., Starkweather, S. M., and Shiobara, M.: Clouds at Arctic atmospheric observations. Part II: Occurrence and macro-physical properties, J. Appl. Meteorol. Clim., 50, 626–644, 2011.

Smith, R. N. B.: A scheme for predicting layer clouds and their water content in a general circulation model, Q. J. Roy. Meteorol. Soc., 116, 435–460, 1990.

Soloman, A., Morrison, H., Persson, O., Shupe, M. D., and Bao, J.-W.: Investigation of the microphysical parameterizations of snow and ice ice Arctic clouds during M-PACE through model-observation comparisons, Mon. Weather Rev., 137, 3110–3127, 2009.

Solomon, A., Shupe, M. D., Persson, P. O. G., and Morrison, H.: Moisture and dynamical interactions maintaining decoupled Arctic mixed-phase stratocumulus in the presence of a humidity inversion, Atmos. Chem. Phys., 11, 10127–10148, doi:10.5194/acp-11-10127-2011, 2011.

Solomon, S., Qin, D., Manning, M., M., M., Averyt, K., Tignor, M. M. B., Miller, H. L., and Chen, Z. (eds.): Climate Change 2007: The Physical Science Basis, IPCC, Cambridge University Press, Cambridge, UK, 2007.

Staniforth, A., White, A., Wood, N., Thuburn, J., Zerroukat, M., Cordero, E., and Davies, T.: Joy of UM 6.3 Model Formulation, Unified Model Documentation Paper, No. 15, Met Office, Exeter, UK, 2006.

Stevens, B., Beljaars, A., Bordoni, S., Halloway, C., Köhler, M., Krueger, S., Savic-Jovcic, V., and Zhang, Y.: On the structure of the lower troposphere in the summertime stratocumulus regime of the Northeast Pacific, Mon. Weather Rev., 135, 985–1005, 2007.

Title Page

Abstract | Introduction

Conclusions | References

Tables | Figures

◀ | ▶

◀ | ▶

Back | Close

Full Screen / Esc

Printer-friendly Version

Interactive Discussion

Tjernström, M.: Is there a diurnal cycle in the summer cloud-capped Arctic boundary layer?, J. Atmos. Sci., 64, 3970–3986, 2007.

Tjernström, M. and Graversen, R. G.: The vertical structure of the lower Arctic troposphere analysed from observations and the ERA-40 reanalysis, Q. J. Roy. Meteorol. Soc., 135, 431–443, 2009.

Tjernström, M. and Mauritsen, T.: Mesoscale variability in the summer Arctic boundary layer, Bound.-Layer Meteorol., 130, 383–406, 2009.

Tjernström, M., Leck, C., Persson, O., Jensen, M., Oncley, S., and Targino, A.: The Summertime Arctic Atmosphere. Meteorological measurements during the Arctic Ocean Experiment 2001, B. Am. Meteorol. Soc., 84, 1305–1321, 2004.

Tjernström, M., Sedlar, J., and Shupe, M. D.: How well do regional climate models reproduce radiation and clouds in the Arctic?, J. Appl. Meteorol. Clim., 47, 2405–2422, 2008.

Tjernström, M., Birch, C. E., Brooks, I. M., Leck, C., Mauritsen, T., Paatero, J., Persson, O., Sedlar, J., Shupe, M. D., Szczodrak, M., and Wheeler, C. R.: Central Arctic atmospheric conditions during the Arctic Summer Cloud Ocean Study (ASCOS) field phase: contrasting to previous expeditions, submitted to Atmos. Chem. Phys., 2011.

Uttal, T., Curry, J. A., McPhee, M. G., Perovich, D. K., Moritz, R. E., Maslanik, J. A., Guest, P. S., Stern, H. L., Moore, J. A., Turenne, R., Heiberg, A., Serreze, M. C., Wylie, D. P., Persson, O. G., Paulson, C. A., Halle, C., Morison, J. H., Wheeler, P. A., Makshtas, A., Welch, H., Shupe, M. D., Intrieri, J. M., Stamnes, K., Lindsey, R. W., Pinkel, R., Pegau, W. S., Stanton, T. P., and Grenfeld, T. C.: Surface heat budget of the Arctic Ocean, B. Am. Meteorol. Soc., 83, 255–275, 2002.

Walsh, J., Kattsov, V., Chapman, W., Govorkova, V., and Pavlova, T.: Comparison of arctic climate simulations by uncoupled and coupled global models, J. Climate, 15, 1429–1446, 2002.

Westwater, E. R., Han, Y., Shupe, M. D., and Matrosov, S. Y.: Analysis of integrated cloud liquid and precipitable water vapour retrievals from microwave radiometers during SHEBA, J. Geophys. Res., 106, 32019–32030, 2001.

Wilson, D. R. and Ballard, S. P.: A microphysically based precipitation scheme for the UK Meteorological Office Unified Model, Q. J. Roy. Meteorol. Soc., 125, 1607–1636, 1999.

Wyant, M. C., Wood, R., Bretherton, C. S., Mechoso, C. R., Bacmeister, J., Balmaseda, M. A., Barrett, B., Codron, F., Earnshaw, P., Fast, J., Hannay, C., Kaiser, J. W., Kitagawa, H., Klein, S. A., Köhler, M., Manganello, J., Pan, H.-L., Sun, F., Wang, S., and Wang, Y.: The

Title Page

Abstract | Introduction

Conclusions | References

Tables | Figures

◄ | ►

◄ | ►

Back | Close

Full Screen / Esc

Printer-friendly Version

Interactive Discussion

PreVOCA experiment: modeling the lower troposphere in the Southeast Pacific, Atmos. Chem. Phys., 10, 4757–4774, doi:10.5194/acp-10-4757-2010, 2010.
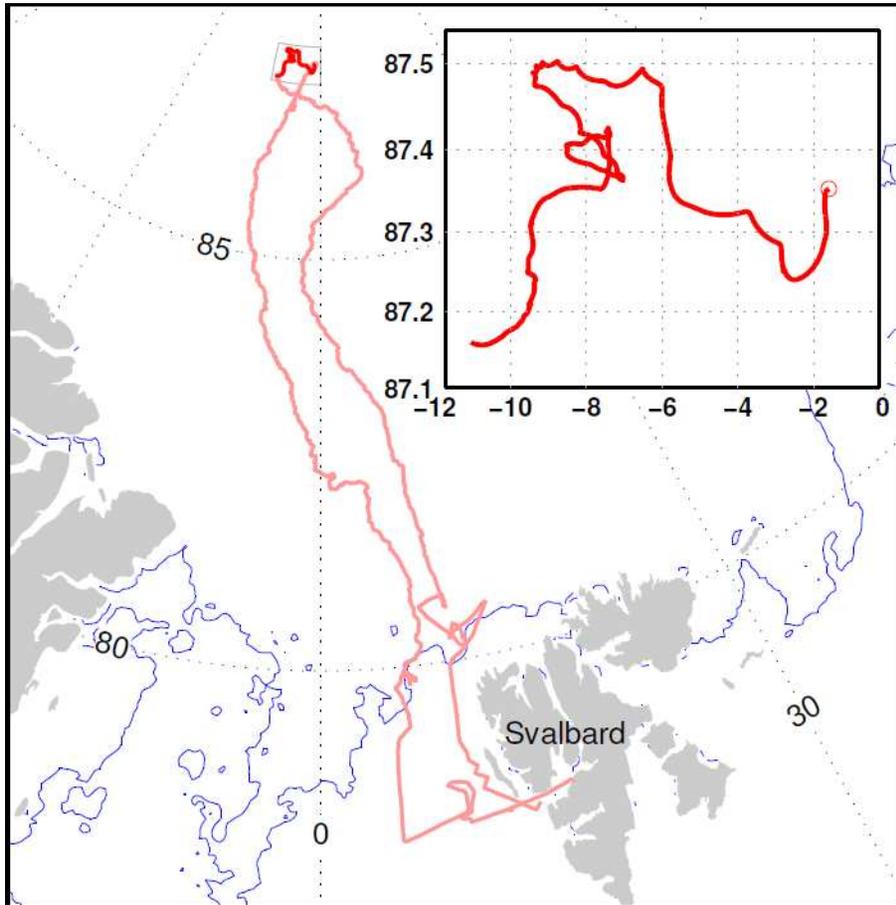
Fig. 1. Map of the ASCOS cruise track (pink) and ice drift (red). The blue line represents the approximate maximum southerly sea ice extent on 12 August 2008 (DoY 225). The insert shows the position of the icebreaker during the ice drift, where the red circle is the start position.
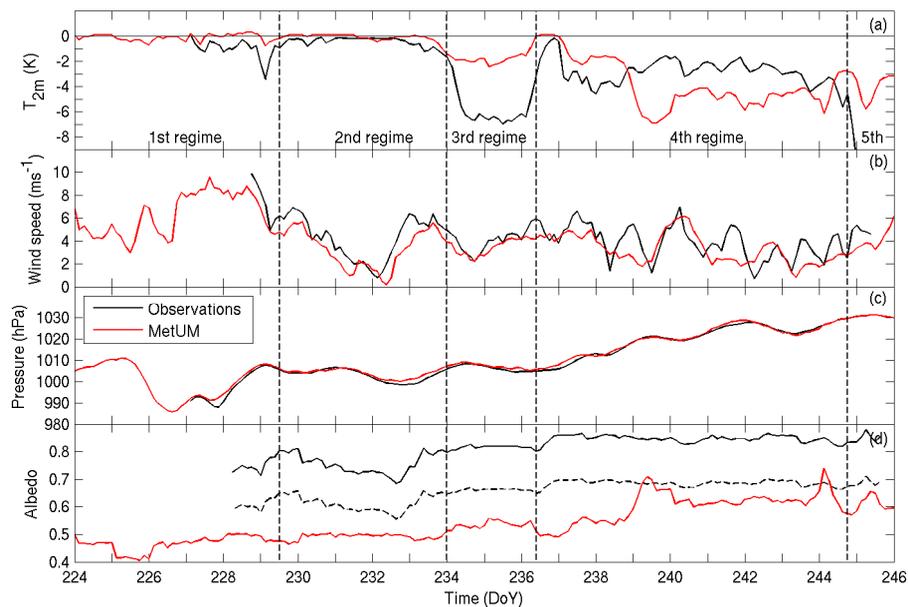
Fig. 2. 3-hourly averaged **(a)** near-surface air temperature, **(b)** wind speed, **(c)** pressure and **(d)** albedo observations and diagnostics from the MetUM, as a function of time (DoY, day of the year). DoY 226 is 13 August 2008. The dashed line in **(d)** represents an estimate of the spatially averaged surface albedo. The vertical dashed lines represent the boundaries between the five temperature regimes.
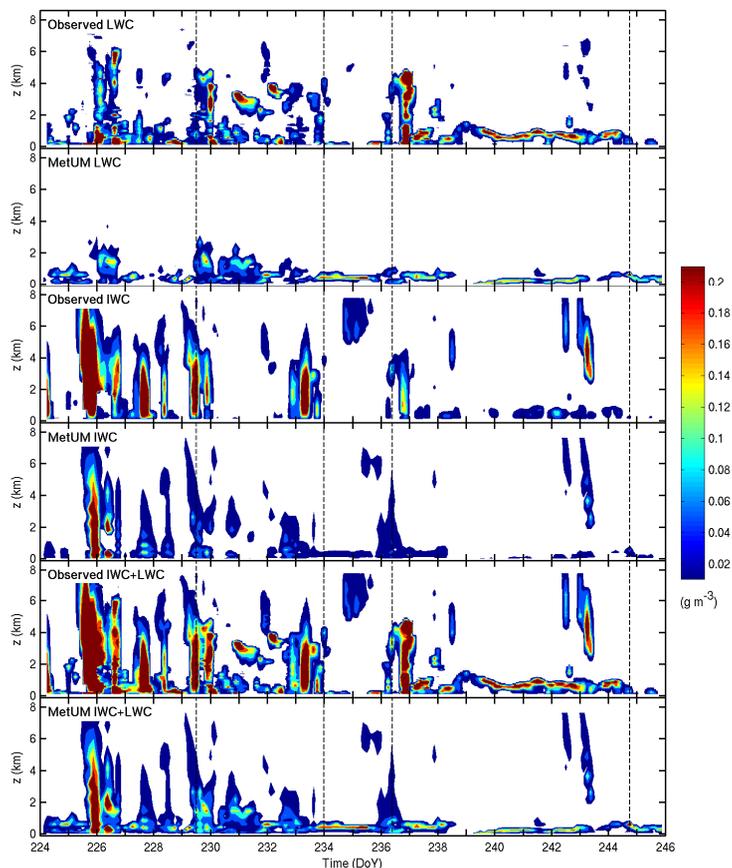
Fig. 3. 3-hourly averaged liquid, ice and total cloud water concentrations observed during ASCOS and diagnostics from the MetUM. The observations are a product derived from measurements made by the remote sensing instruments. The vertical dashed lines represent the boundaries between the five temperature regimes.

Back | Close

Full Screen / Esc

Printer-friendly Version

Interactive Discussion
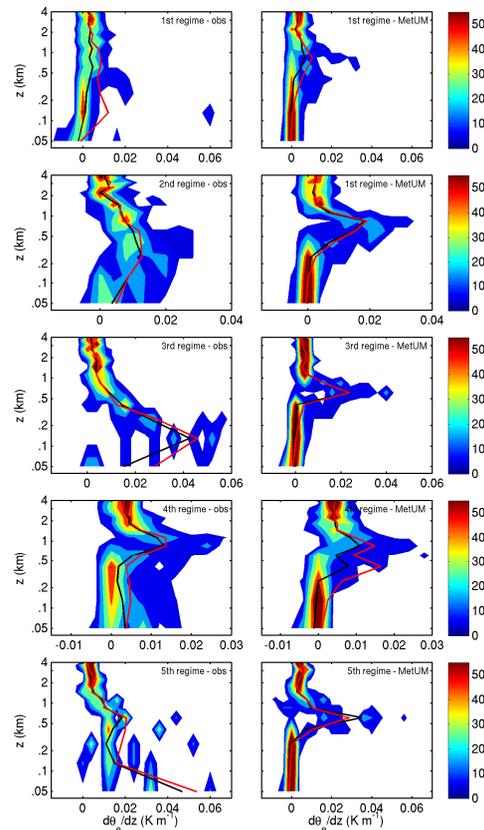
Fig. 4. Contours of the probability of static stability, given by the vertical derivative of equivalent potential temperature ($\partial\theta_e/\partial z$), as a function of height. Observations are from the 6-hourly soundings and the model data are from 3-hourly diagnostics. The red and black lines are the mean and median static stability at each vertical level, respectively. Note the logarithmic height scale and the change in scale on the *x* axis.
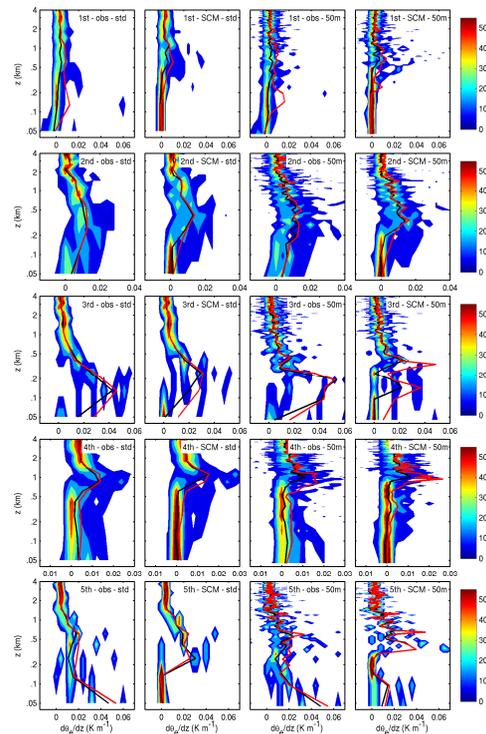
Fig. 5. Contours of the probability of static stability, given by the vertical derivative of equivalent potential temperature ($\partial \theta_e / \partial z$), as a function of height for the single-column model run initialised with observed surface temperature. The first and third columns show observations from the 6-hourly soundings for each regime, averaged onto the standard and 50 m vertical resolutions of the SCM, respectively. The second and fourth columns show SCM diagnostics at $t + 6$ h, run at standard and 50 m vertical resolution, respectively. The red and black lines are the mean and median static stability at each vertical level, respectively. Note the logarithmic height scale and the change in scale on the x axis.

Full Screen / Esc

Printer-friendly Version

Interactive Discussion
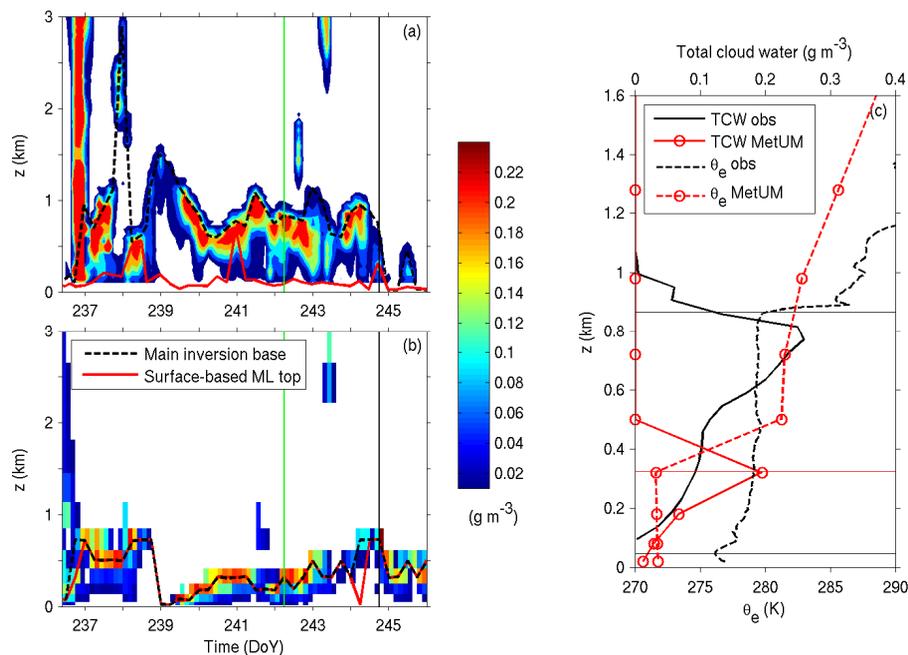
Fig. 6. Total cloud water concentrations: **(a)** 3-hourly averaged observations and **(b)** 3-hourly operational diagnostics from the MetUM. The black dashed line shows the base of the main inversion and the red line shows the top of the surface-based mixed layer. The vertical black line represents the start of the 5th regime and the vertical green line indicates the time of the data used in **(c)**. Panel **(c)** shows the observed (black lines) and modelled (red lines) total cloud water content and equivalent potential temperature (θ_e) at DoY 242.25. The horizontal lines show the heights of the main inversion base and of the surface-based mixed layer top.
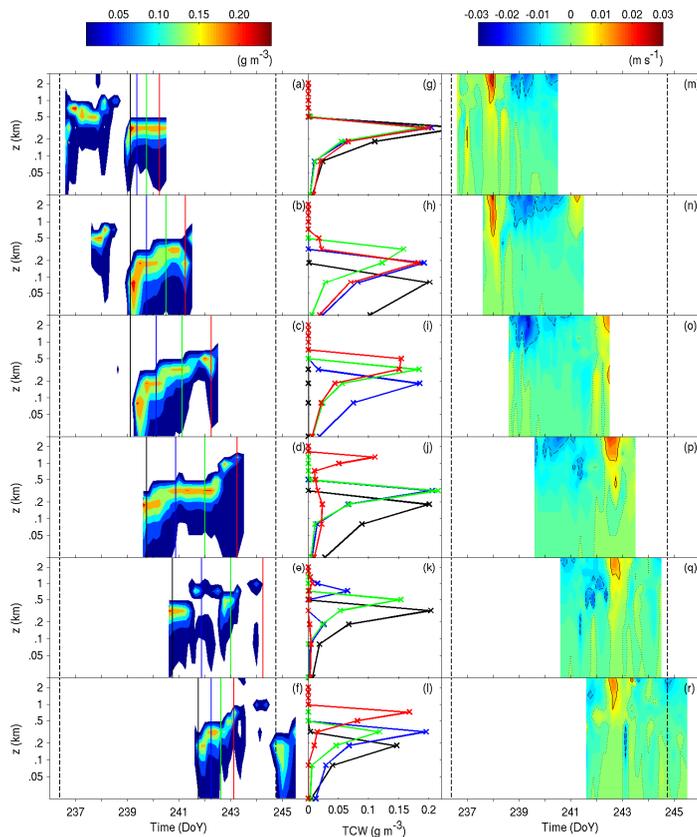
Fig. 7. Total cloud water concentrations (panels **a** to **f**), total cloud water profiles (**m** to **r**) and vertical velocity (**g** to **l**) for six 4-day operational forecasts, initialised daily at 12:00 UTC. The colours of the total cloud water concentration profiles in panels **(g)** to **(l)** relate to the times marked by the coloured lines in panels **(a)** to **(f)**. Note the logarithmic y-axis scale on all panels.
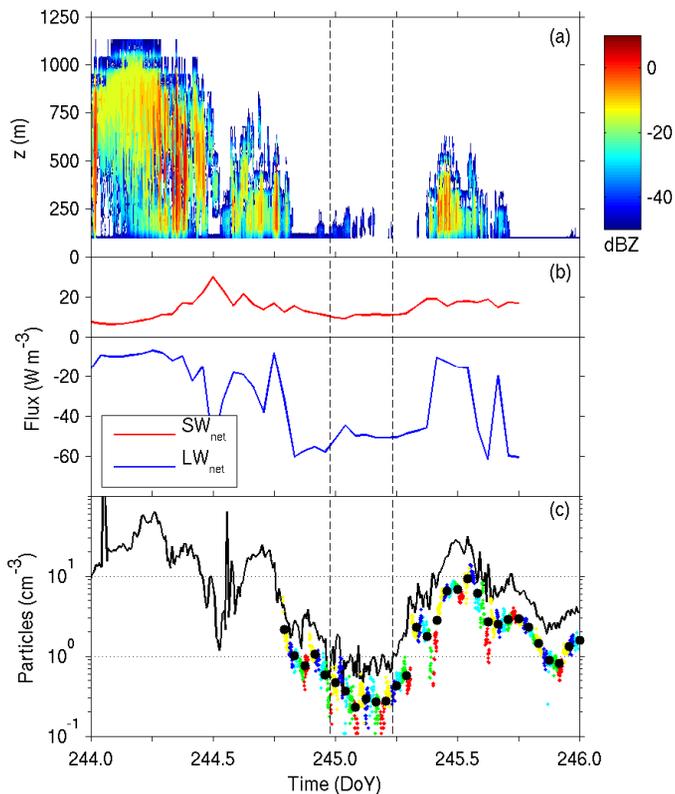
Fig. 8. Cloud and aerosol observations from the 5th regime **(a)** radar reflectivity, **(b)** observed net shortwave and longwave radiative fluxes and **(c)** accumulation mode particle (60 nm < diameter <800 nm) concentration from the DMPS (black line) and mean CCN concentration (black dots), computed from measurements made at a range of supersaturations (coloured dots, red 0.11 %, green 0.16 %, cyan 0.21 %, blue 0.42 % and yellow 0.73 %). The vertical dashed lines show the times of the two radiosondes used in the SCM runs in Figs. 9–11.
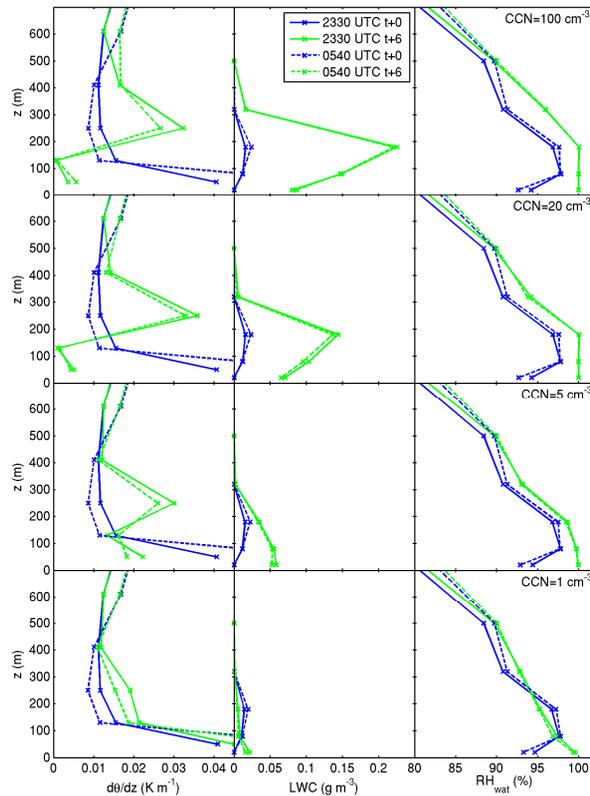
Fig. 9. Static stability, cloud liquid water concentration and relative humidity from the SCM. The model was initialised at 23:30 UTC, DoY 244 (solid lines) and 05:40 UTC, DoY 245 (dashed lines), using radiosonde profiles. The upper panel shows results from the control run, where CCN = 100 cm^{-3} and the lower panels shows results from experiments, where CCN = 20, 5 and 1 cm^{-3}. The blue and green colours represent the SCM diagnostics at $t + 0$ and $t + 6$ h, respectively.
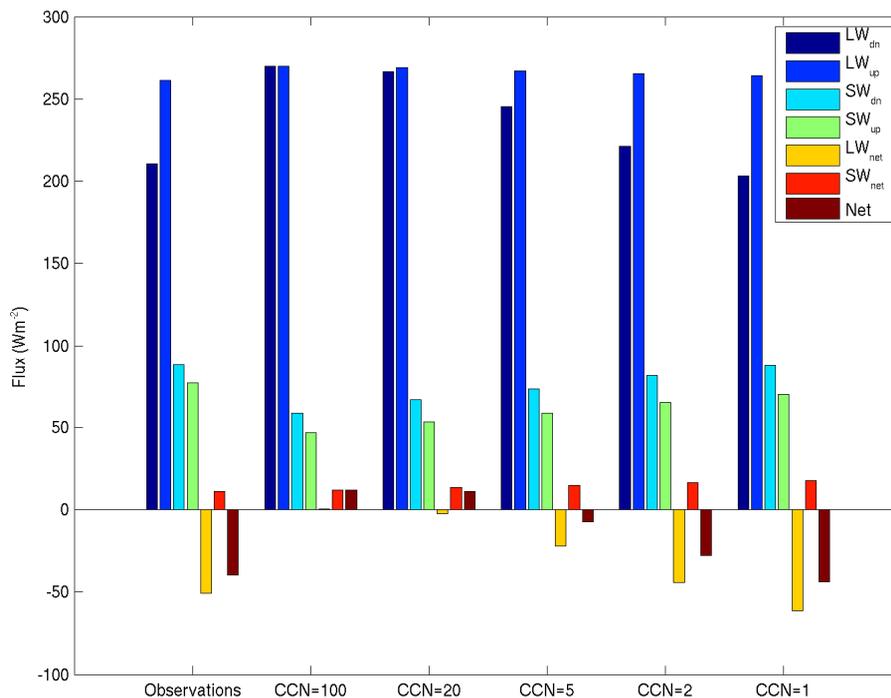
Fig. 10. Mean radiative flux observations between 05:00 and 06:00 UTC, DoY 245 and radiative flux diagnostics at $t + 6$ h from the SCM run initialised at 23:30 UTC, DoY 244.

Title Page

Abstract | Introduction

Conclusions | References

Tables | Figures

◄ | ►|

◄ | ►

Back | Close

Full Screen / Esc

Printer-friendly Version

Interactive Discussion
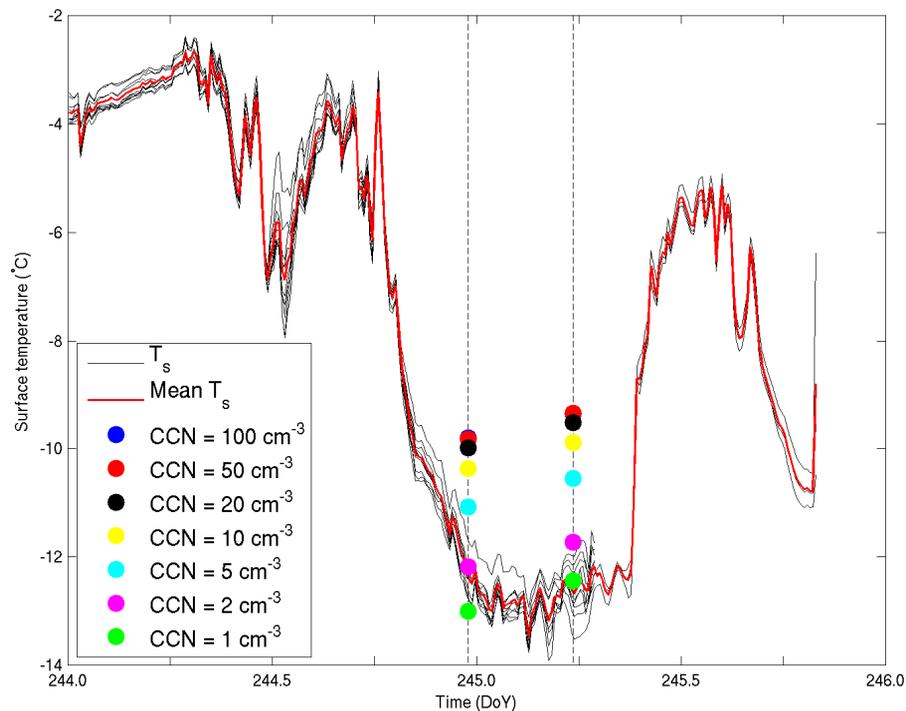
Fig. 11. Surface temperature observations from 10 different thermocouples (faint black lines), and their mean (red line). The coloured dots show surface temperature from the SCM experiments with various CCN concentrations.

ASCOS case studies

C. E. Birch et al.